

Provided for non-commercial research and education use.
Not for reproduction, distribution or commercial use.



This article appeared in a journal published by Elsevier. The attached copy is furnished to the author for internal non-commercial research and education use, including for instruction at the authors institution and sharing with colleagues.

Other uses, including reproduction and distribution, or selling or licensing copies, or posting to personal, institutional or third party websites are prohibited.

In most cases authors are permitted to post their version of the article (e.g. in Word or Tex form) to their personal website or institutional repository. Authors requiring further information regarding Elsevier's archiving and manuscript policies are encouraged to visit:

<http://www.elsevier.com/copyright>



Contents lists available at ScienceDirect

Combustion and Flame

www.elsevier.com/locate/combustflame

Combustion characteristics of boron nanoparticles

Gregory Young, Kyle Sullivan, Michael R. Zachariah*, Kenneth Yu

AJC School of Engineering, University of Maryland, College Park, MD 20742, USA

ARTICLE INFO

Article history:

Received 19 February 2008

Received in revised form 8 October 2008

Accepted 10 October 2008

Available online 4 December 2008

Keywords:

Boron

Nanoparticles

ABSTRACT

An experimental investigation of the combustion characteristics of boron nanoparticles in the post flame region of a flat flame burner has been conducted. Boron is attractive as a fuel or a fuel supplement in propellants and explosives due to its high heats of combustion on both a gravimetric and volumetric basis. A relatively large database exists for combustion characteristics of large (greater than 1 μm) boron particles, but very little exists for nano-sized boron. Ignition and combustion characteristics have been studied in the post flame region of a fuel lean $\text{CH}_4/\text{Air}/\text{O}_2$ flame, with burner temperatures ranging from about 1600 K to 1900 K, and oxygen mole fractions ranging between 0.1 and 0.3. As in earlier investigations on boron combustion, a two-stage combustion phenomenon was observed. Ensemble-averaged burning times of boron nanoparticles were obtained, while the ignition time measurements for boron nanoparticles were extended into a lower temperature range previously unavailable in the literature. The measured burning times were between 1.5 ms and 3.0 ms depending on both the temperature and oxygen mole fraction. The ignition times were relatively insensitive to oxygen concentration in the range studied, and were affected only by temperature. The measured ignition times were inversely related to the temperature, ranging from 1.5 ms at 1810 K to 6.0 ms at 1580 K. The burning time results were compared to both diffusion and kinetic limited theories of particle combustion. It was found that the size dependence on particle burning times did not follow either theory.

© 2008 The Combustion Institute. Published by Elsevier Inc. All rights reserved.

1. Introduction

Metal additives are common in solid rocket propellants and explosives due to their ability to increase energy density. In particular boron has been studied for many years because it has the highest volumetric heating value of any element. Although boron exhibits exceptional performance characteristics, it has rarely achieved its potential in propulsion systems. Ulas and Kuo [1] suggest there are two major reason for this; (1) the ignition of boron particles is significantly delayed due to the presence of an oxide layer on the particle surface, and (2) the energy release during the combustion process of boron particles in hydrogen containing gases is significantly lowered due to the formation of HBO_2 . Early studies on boron particle combustion by Macek and Semple [2–4] describe a two-stage combustion process. The first stage is associated with particle burning while the particle is still coated with an oxide layer. As the particle heats up to above the B_2O_3 boiling point and the oxide layer is completely removed by evaporation, the second stage of boron combustion begins. Since pure boron has relatively high melting and boiling temperatures, 2350 K and 4139 K respectively, the initial reactions in the consumption of the boron particle involve heterogeneous reactions between the gas phase oxidizer

and solid or liquid phase boron. The second stage is essentially the standard combustion of the bare boron particle. Therefore, the removal of the liquid oxide layer plays an important role in the ignition and combustion of boron [5]. Numerous studies [2,6,7] involving micron-sized and larger boron identified a critical ignition temperature ranging between about 1500 K and 1950 K in oxygenated environments. Dreizin et al. [8] suggest that the ignition event at these temperatures could be associated with polymorphic phase transitions of the boron particle.

Several studies [9–11] found that the presence of water vapor greatly enhanced boron oxide gasification rates. In addition, hydrogen-containing species can accelerate the gas-phase combustion process [12]. Unfortunately the presence of water vapor promotes the formation of HBO_2 , which is thermodynamically favored over gaseous B_2O_3 as the temperature is lowered. This results in the boron being “trapped” as HBO_2 and therefore not releasing all of its energy. This “energy trap” arises from the fact that from an energetic standpoint, the best product of boron combustion is liquid phase $\text{B}_2\text{O}_3(l)$.

Yeh and Kuo [5] showed that when the combustion process is limited by diffusion, the combustion rate is governed by a D^2 -law, while the combustion rate is governed by a D^1 -law when the combustion process is limited by kinetics. They suggest that the dominant mechanism can be determined by evaluation of the Damköhler number, and that large particles at high pressures ex-

* Corresponding author.

E-mail address: mrz@umd.edu (M.R. Zachariah).

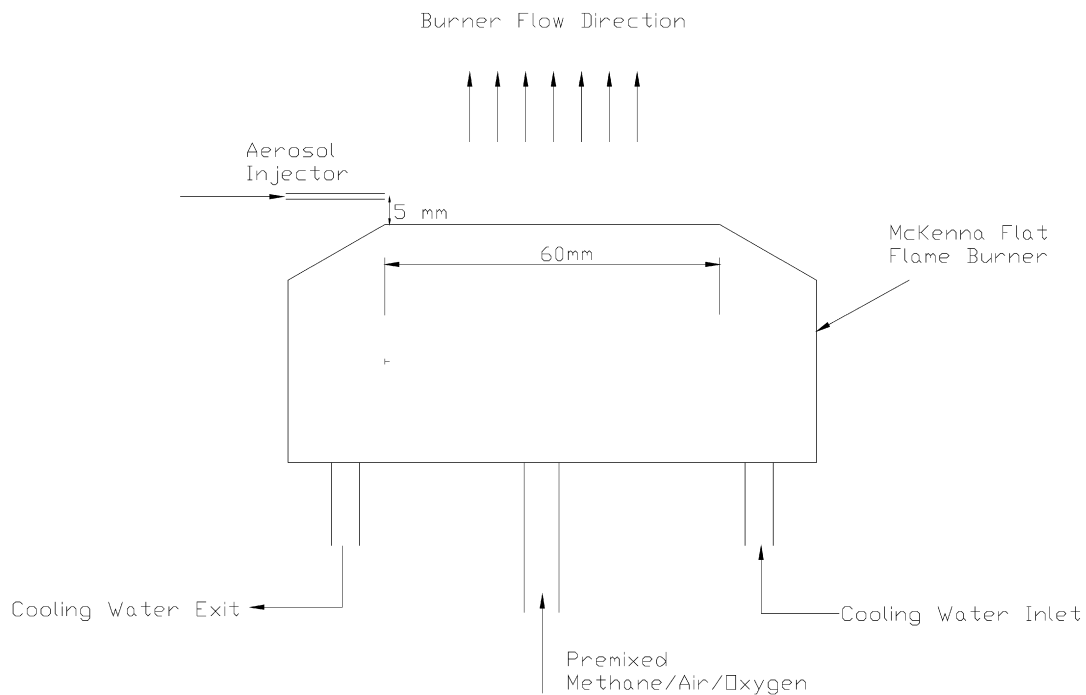


Fig. 1. Schematic diagram of burner and injection scheme.

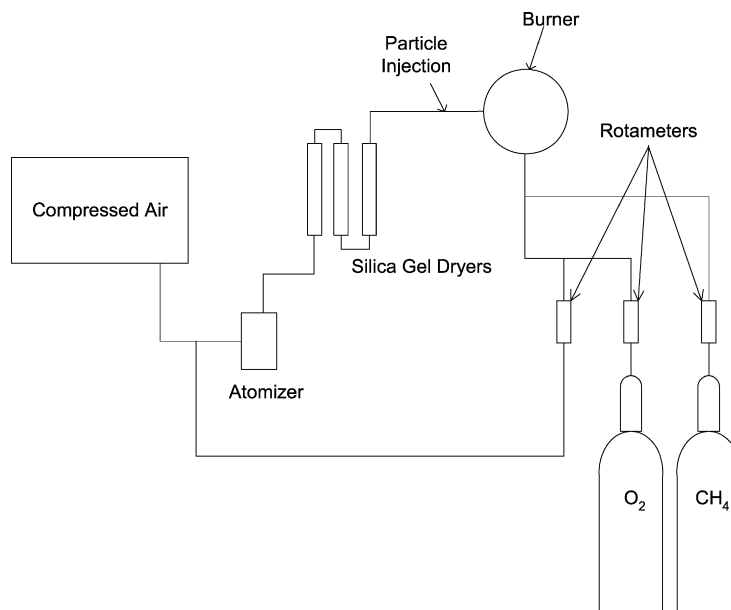


Fig. 2. Schematic diagram of burner test setup.

Stokes number was less than unity in each case the droplets were considered suitable seed particles for the experiment.

$$S_{\text{particle}} = \frac{\rho_p D^2 U}{18\mu} \quad (1)$$

By matching the momentum flux ratios we have ensured that the fluid in the jet will follow the same trajectory in both the hot and cold flow. A small Stokes number ensures that the particles will follow the carrier gases very closely. Considering the current experiment and a conservative estimate of 1000 nm for our largest boron particle size, in a worst case scenario the particles have a Stokes number of 0.02. Therefore, we can be assured that not only are the water droplets suitable seed particles for the PIV experiments, but our boron particles were also subjected to the same

momentum flux ratio and were able to follow the carrier gas just as well as the water droplets.

For the experiments an LA Vision PIV setup was employed. This includes an ND:Yag laser and an ICCD camera. The laser sheet was passed through the injector flow and the camera was placed perpendicular to the laser sheet. For data processing, the standard PIV sum of correlation was used. In total three different injection flow rates were studied under 12 different burner crossflows. Fig. 3 shows an example of a collected image pair. For each test condition, 50 images were collected and processed to determine the velocity vectors, an example of which can be seen in Fig. 4. Since the data collection for this study results in spatial locations of the boron combustion process, only the axial-component of velocity was important in later data analysis. Fig. 5 shows the averaged

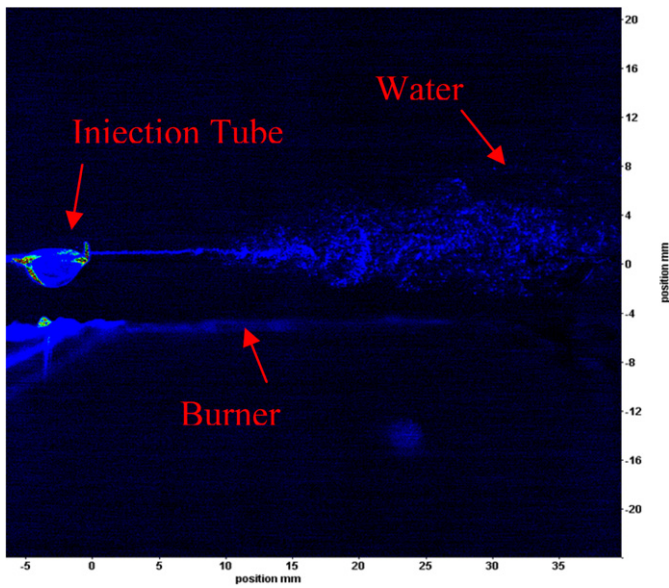


Fig. 3. Image pair collected in PIV experiment.

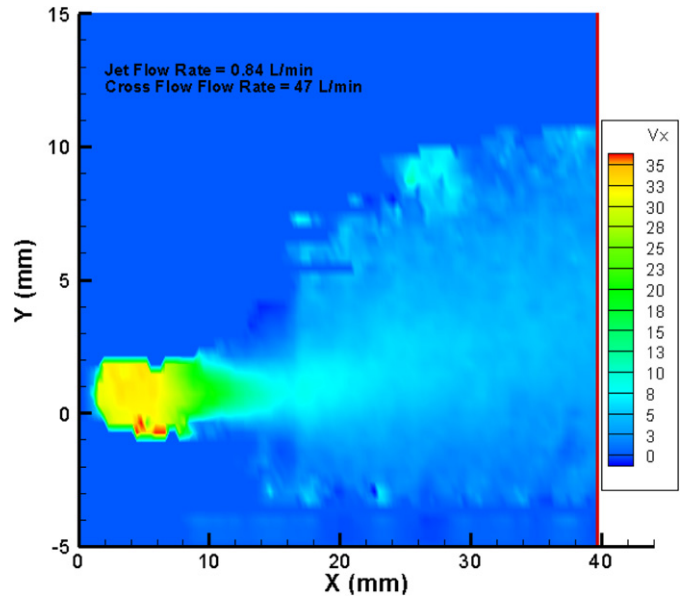


Fig. 5. Average axial-component of velocity.

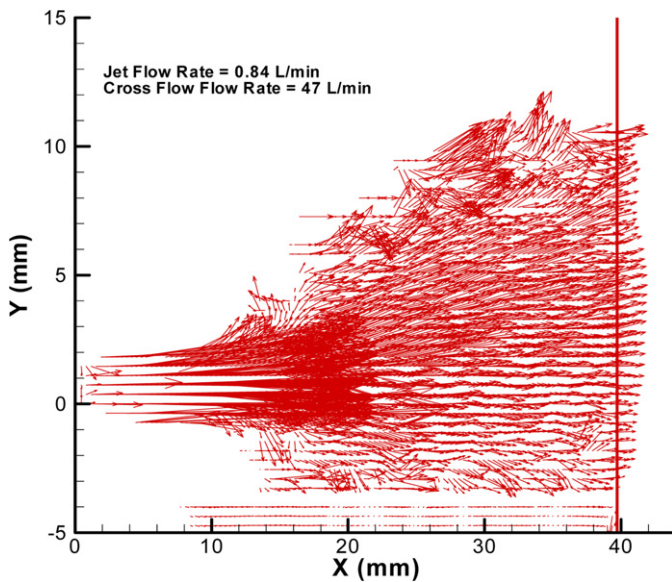


Fig. 4. Velocity vectors obtained using PIV.

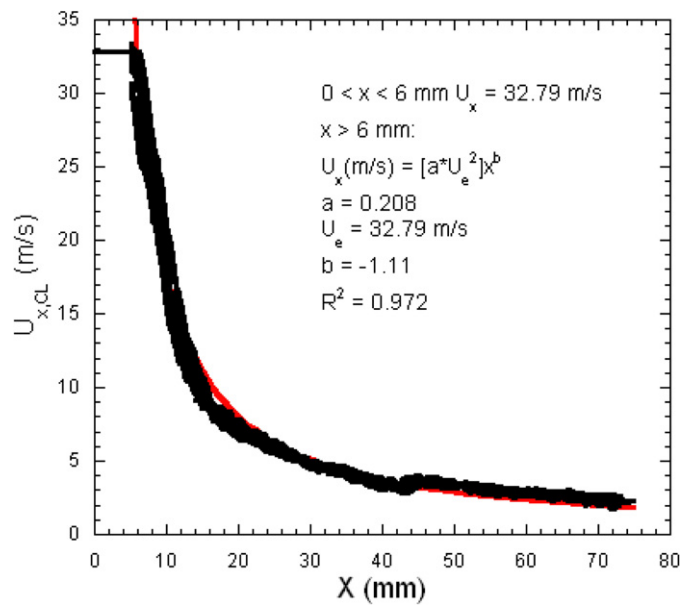


Fig. 6. Correlation for centerline jet velocity.

axial-component of velocity for the selected injection flow rate under the highest crossflow condition used in this experiment. The centerline velocity was extracted from all of the experiments and plotted in Fig. 6, which shows that under these conditions, the crossflow does not significantly affect the centerline velocity. The location of the centerline does change, but the magnitude of the centerline velocity at a given axial location does not vary by significant amounts with changing crossflow.

An analytical expression to describe the centerline axial component of velocity can be derived based upon a laminar jet exhausting into a quiescent atmosphere. The expression is seen in Eq. (2). Using this expression for guidance, a correlation was extracted to provide one velocity profile for all crossflows in subsequent data analysis. Therefore the centerline velocity may be represented by a piecewise function. For the first 6 mm from the injection location, the velocity is a constant determined by taking the average of all of the maximum velocities collected for a given injection flow rate. After 6 mm the correlation is used to represent the velocity of the particles. This piecewise function is illustrated in Fig. 6.

$$u_{x,CL} \text{ (m/s)} = [a u_e^2] x^b \quad (2)$$

The solution for a jet exhausting into a quiescent atmosphere has an exponent, b , equal to -1 . The results obtained here in a moderate crossflow, show a spatial dependence $u_{x,CL} \sim x^{-1.11}$, which is relatively consistent with the quiescent atmosphere solution.

2.3. Particle characterization

SB99 boron particles were obtained from the SB Boron Corporation and used in all of the combustor testing during this study. As previously mentioned, most boron particles contain some oxide layer on the outside of the particles. When nanoparticles are considered, even a small oxide layer may be a significant portion of the total mass/volume of the particle. This layer not only impedes combustion, but also essentially removes the available energy from a given particle. In order to estimate how much of the boron particle is occupied by the oxide layer; a thermal gravimetric analysis (TGA) was performed. The TGA was conducted in a

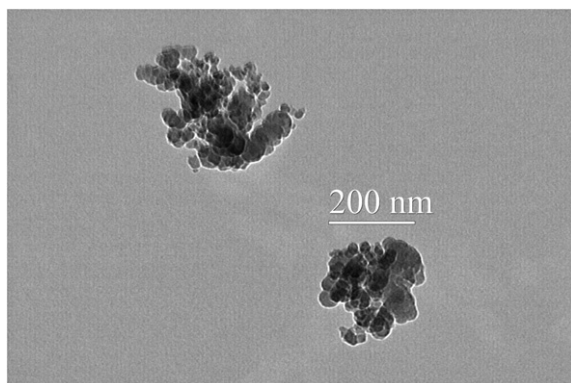


Fig. 7. TEM image at particle injection location.

50% oxygen/50% argon environment with a heating rate of 5 °C per minute. Essentially, the assumption is that the available boron undergoes complete oxidation since it is in an oxygen environment. Therefore the mass added to the sample during oxidation is exclusively the result of oxygen reacting with the boron [17]. Knowing the stoichiometric ratio and the mass gained during the test, one can deduce the amount of active boron in the sample. From the TGA results, the elemental boron content in the SB99 particles was found to be 72.2% by mass.

Yang et al. suggest that the primary particle size of the SB99 particles is 62 nm [18]. In this study however, the particles tended to be quite agglomerated. The particles were added to distilled water to create a solution for atomization. In order to understand the size distribution of the particles as they were injected into the post flame region, two different measurements were made. The first measurement, while not entirely quantitative allowed for visualization of the condition of the particles as they entered the burner and was made by transmission electron microscopy (TEM). The particles were collected at the end of the injection system, as they would be when injected into the post flame region during the actual experiment. Fig. 7 is a representative TEM image. As was mentioned earlier, the image reveals that the particles that were injected are in fact agglomerations of smaller primary particles. In general the agglomerations we observed through TEM were approximately 200 nm in size.

The second measurement to understand the size distribution utilized a commercial differential mobility analyzer (DMA) [19] purchased from TSI Inc. This device serves to construct a size distribution in a polydisperse aerosol by electrostatically separating particles by mobility size and then recording the concentration by means of a condensation particle counter (CPC). This method allows for a very sensitive (<1 nm resolution) online sampling of an aerosol. The boron particles were redirected at the injection location for sampling and Fig. 8 shows the size distribution determined by the DMA. The results indicate that the mean mobility diameter of the “particles” was approximately 200 nm. In other words, the “particles” behaved aerodynamically as a spherical particle of 200 nm in diameter. Unfortunately, the range of the DMA truncated the measurement to less than 500 nm. According to Friedlander [20], aerosol size distributions often have large standard deviations caused by a long upper “tail” for particles larger than the peak in the distribution. Such distributions can be represented approximately by the lognormal distribution function:

$$n_d(D_p) = \frac{N_\infty}{(2\pi)^{1/2} D_p \ln \sigma_g} \exp \left[-\frac{(\ln D_p - \ln d_{pg})^2}{2 \ln^2 \sigma_g} \right], \quad (3)$$

where N_∞ refers to the total concentration of particles at a given point and time, d_{pg} refers to the geometric mean diameter, and σ_g refers to the geometric standard deviation. Equation (3) was used

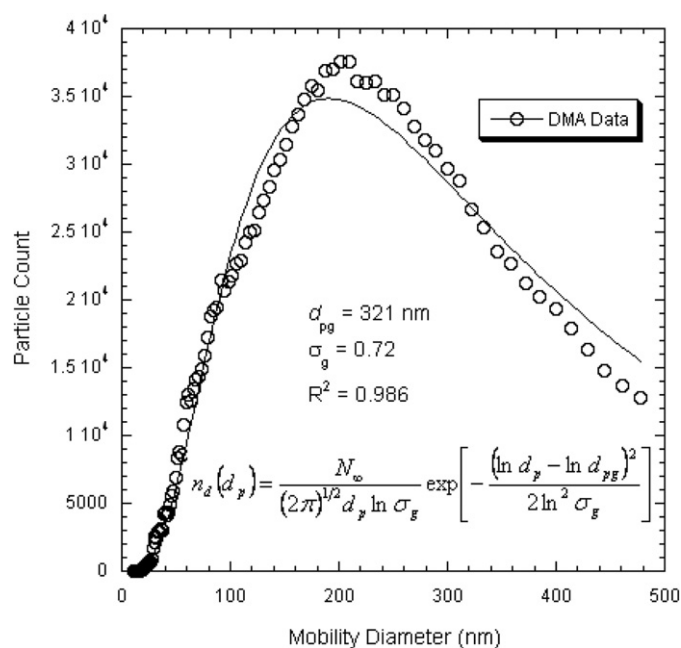


Fig. 8. Size distribution determined by DMA.

to fit the data collected by the DMA and used to extrapolate the aerosol properties during data processing. The curve fit can be seen in Fig. 8 along with the original DMA data.

2.4. Test conditions

A mixture of methane/air/oxygen created the environment used to study the ignition and combustion characteristics of the SB99 nanoparticles. B-type (platinum/rhodium) thermocouples were used to measure the temperature of the flat flame burner under steady state conditions. Measurements were made at three locations, $x = 10, 30, 50$ mm, from the injection source 5 mm above the burner surface. The measurements were corrected for radiation loss. The method for correction is the same as explained in Ref. [21]. After correction, the three measurements were averaged together for data analysis purposes. The test matrix for this study as well as the results of the temperature measurements can be seen in Table 1. The measured temperatures were considerably below the adiabatic flame temperatures for a given condition. This is primarily a result of significant heat loss to the water-cooled burner. Under the conditions considered in this study, the burner temperature was fairly insensitive to equivalence ratio; rather the temperature was driven by fuel flow rate. A similar finding was observed using this burner in Refs. [22,23]. The product mole fractions listed in Table 1 represent the nominal values based upon complete combustion of the fuel.

3. Results and discussion

A Cooke Dicom Pro intensified CCD camera (ICCD) with a minimum shutter speed of 1 ms and typical framing rates around 11 Hz was used to visualize the combustion properties of the SB99 particles. Similar to previous observations, when appropriate temperature and or burner product composition requirements were met, a two-stage combustion phenomenon was observed, which is consistent with observations from other researchers [2,24]. Initially, as the particles were injected into the post flame region, there was no visible phenomenon occurring. Further downstream, a yellowish/orange region appeared for some duration and if appropriate burner conditions were met, the yellowish region was

Table 1
Test conditions.

Test condition	Volumetric flow rates (L/min)			Product mole fractions				Average burner temperature (K)
	O ₂	Air	CH ₄	O ₂	H ₂ O	CO ₂	N ₂	
1	16.8	30.2	5.8	0.200	0.234	0.117	0.450	1684
2	21.0	29.8	7.3	0.200	0.266	0.133	0.400	1808
3	24.8	27.5	8.7	0.200	0.300	0.150	0.350	1854
5	28.6	24.5	10.1	0.200	0.234	0.117	0.450	1637
6	23.2	30.2	5.6	0.300	0.200	0.100	0.400	1630
7	28.9	29.8	7.3	0.300	0.233	0.117	0.350	1797
8	33.2	26.8	8.8	0.300	0.267	0.133	0.300	1872
9	19.2	24.9	4.6	0.300	0.200	0.100	0.400	1578
10	14.0	26.5	5.8	0.150	0.267	0.133	0.450	1718
11	17.7	33.4	7.3	0.150	0.267	0.133	0.450	1814
13	11.0	20.7	4.5	0.150	0.267	0.134	0.449	1596
14	8.5	28.9	4.5	0.100	0.233	0.117	0.550	1614
15	11.0	28.3	5.6	0.100	0.267	0.134	0.499	1712
16	13.7	35.3	6.9	0.100	0.267	0.134	0.499	1791

followed by an abrupt change to a bright white glow region. Li and Williams [24] concluded that the yellow region can be considered the ignition region, or first stage of boron combustion, culminating in complete removal of the oxide layer, while the white glow region signified full fledged combustion, or the second stage of boron combustion.

In order to extract usable data from the observed phenomenon, two sets of images were taken for each test condition; the first image was an unfiltered image, while the second utilized a narrow-band interference filter, centered at 546 ± 2 nm and had a full width half maximum (FWHM) value of 10 nm. In each case 50 images were collected and averaged together for data analysis. In addition, background images were taken, i.e. no particles flowing, and were subtracted from the original averaged images to remove any background emission associated with hydrocarbon combustion. Typically though, no emission of any significance was detected during the collection of the background images for the camera settings that we employed. 546 nm corresponds to a band of emission for the BO₂ molecule, which is a reactive intermediary gas-phase species, formed throughout boron particle ignition and combustion [25]. Li et al. [26] examined the two-stage combustion behavior of boron particles spectrally. In this study they describe a yellow region, which they attributed to ignition, and a bright green region, which they've attributed to combustion. They found that none of the yellow region contributed to the spectra that they were analyzing in the green region, while they observed broad maxima at several wavelengths with 542 nm being the strongest. Li et al. [26] attributed the peaks of their broad maxima to BO₂ emission. Similarly Spalding et al. [27] studied boron suboxides during ignition and combustion through emission spectroscopy and verified a two stage combustion process in nitrogen containing atmospheres. Spalding et al. [27] also found maxima at multiple wavelengths with the strongest being near 546 nm in atmospheres in which no fluorine was included. This observation is certainly in agreement with that of Li et al. [26] and verifies the idea of a two-stage combustion process.

Fig. 9 shows an unfiltered image of the complete combustion process, while Fig. 10 shows the filtered image where only the second stage of combustion was observed. Fig. 11 shows a series of processed images, as BO₂ intensity contours collected for an oxygen mole fraction, X_{O₂}, of 0.3. This shows the location of stage two combustion and as would be expected as the temperature is increased the location shifts closer to the origin.

Although Spalding et al. [28] suggest that the BO₂ spectrum is readily observable during both the full-fledged combustion and ignition stages of boron combustion, the yellow ignition region was not observed in the filtered images. This does not necessarily suggest that BO₂ was not present, only that the level of emission was

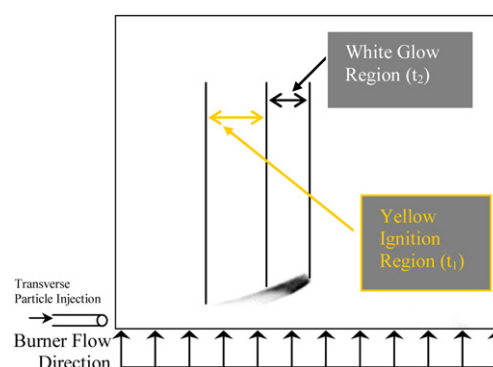


Fig. 9. Unfiltered image of SB99 combustion.

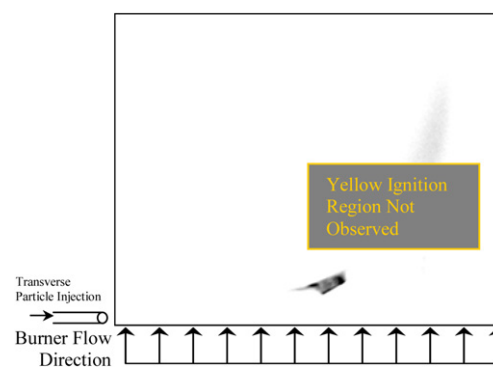


Fig. 10. Filtered image of SB99 combustion.

not strong enough for the camera settings used in the testing. Furthermore, as mentioned earlier Li et al. [26] did not detect any BO₂ emission at a similar wavelengths during the ignition stage. This behavior allowed for a clear distinction between the first and second stage of boron combustion. For data analysis purposes, the filtered images provided the spatial location of stage two combustion. The starting boundary of stage two combustion also served as the ending boundary for stage one combustion. Finally, the unfiltered images gave the starting location for stage one combustion. This was defined as the first instance that visible emission was detected.

In order to verify that BO₂ was being detected and not just black body radiation, an experiment was conducted in which a 532 nm filter replaced the 546 nm filter, since there are no BO₂ bands in the direct vicinity of 532 nm. Fig. 12 shows the emission intensity contours for each filter. The integrated intensity levels for the 546 nm filter image are typically at least 50% higher than

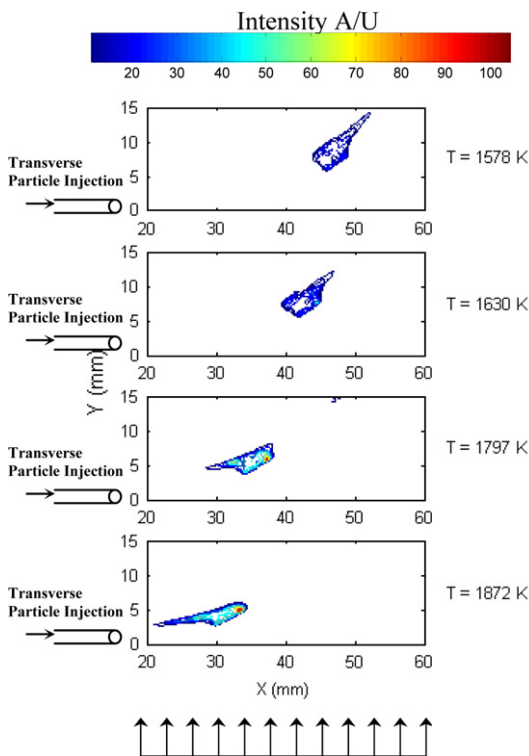


Fig. 11. Sequence of processed images for $X_{O_2} = 0.3$.

the image obtained with the 532 nm filter. If we consider Planck's Law:

$$I_b(\lambda, T) = \frac{C_1/\pi}{\lambda^5(\exp[C_2/(\lambda T)] - 1)}, \quad (4)$$

where $C_1 = 2\pi hc_0^2 = 37,413 \text{ W}\mu\text{m}^4/\text{cm}^2$ and $C_2 = hc_0/k_B = 14,388 \mu\text{mK}$ and integrate the black body radiation intensity over the full width half maximum value (10 nm) of the filter, we find that the black body radiation should be about 35% higher at 546 nm than at 532 nm for 1600 K and about 25% higher at 2000 K. Thus suggesting that the emission detected at 546 nm must be more than just the contribution associated with black body radiation and must be attributed to boron combustion. Furthermore we can rule out the idea of black body radiation further by inspection of the intensity profiles. There is a clear beginning and end luminescence in the filtered images. If we were detecting primarily black body radiation we would expect to continue to see black body radiation after consumption of the boron particles since the products of combustion are primarily condensed phase B_2O_3 at these temperatures. This suggests that while black body radiation certainly would exist in this system, between the camera settings used and the effects of filtering we have minimized its effect on what we have visualized. It should also be noted, that we did not detect any significant emission when particles were absent in the system at either wavelength (532 nm or 546 nm). While hydrocarbon emission would normally be expected at these wavelengths, with the camera settings we employed we did not detect anything of significance. Furthermore, we conducted similar experiments with nano-aluminum and were unable to detect anything above blackbody radiation levels. Therefore, it is reasonable to conclude that the intensity levels detected at 546 nm with the boron particles can be directly attributed to boron combustion processes.

As Fig. 11 shows, the “shape” of the stage two combustion was not consistent for differing test conditions, making the problem two-dimensional and difficult to evaluate. As such, a technique for evaluating the spatial boundaries needed to be developed. Thus,

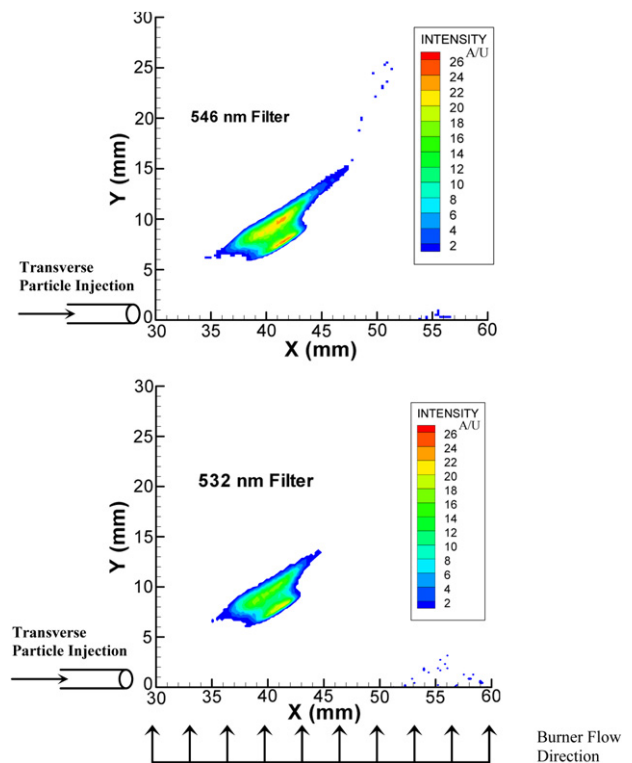


Fig. 12. Intensity contours using different filters.

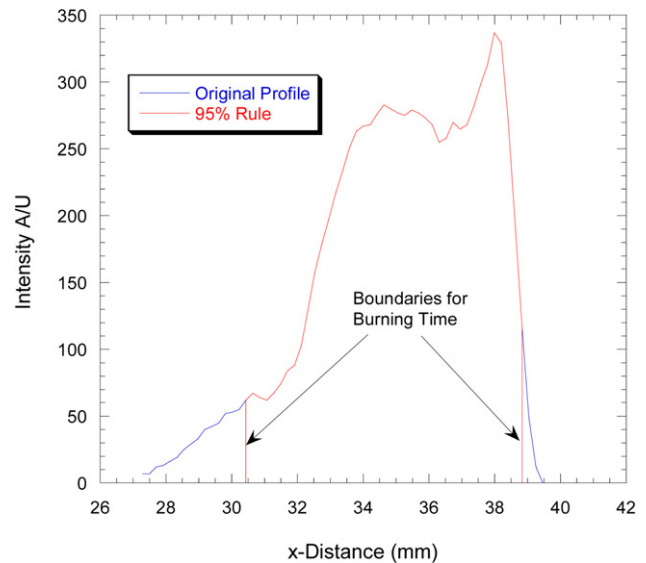


Fig. 13. Example of t_2 burn time determination ($X_{O_2} = 0.2$, $T = 1808 \text{ K}$).

the problem was made one-dimensional by summing the columns of the images (or the y-dimension) and then plotting the profile in the x-direction. Once this was accomplished an area rule was utilized for determining the boundaries of stage two combustion. An area-based method was chosen since area based methods provide the most unambiguous determination of burn time [29]. In this case the burning time was defined as occupying 95% of the area of the original profile as shown in Fig. 13, where the blue line represents the original profile, while the red line represents 95% of the total area, and therefore the burning time. The boundary on the left side of Fig. 13 identifies the start of stage two combustion and the end of stage one combustion. Therefore, with spatial locations of the beginning and ending of each stage of combustion, and the velocity measurements, the ensemble average

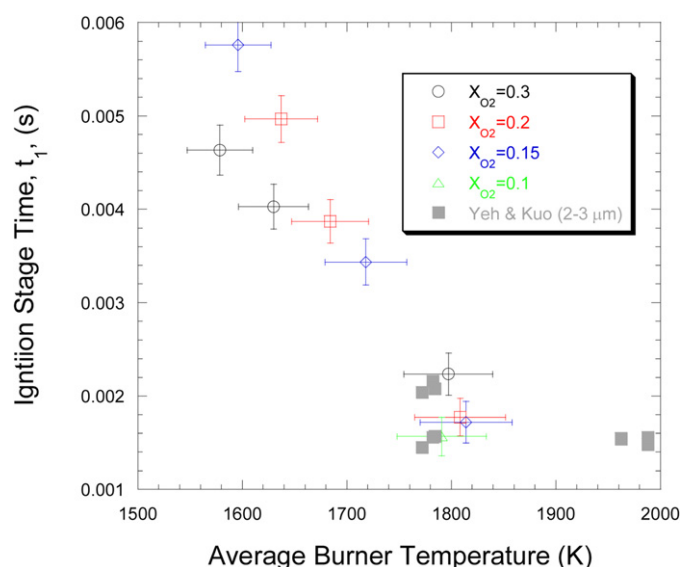


Fig. 14. t_1 ignition stage times.

ignition and combustion times of the SB99 particles can now be extracted.

Fig. 14 shows the results of the stage one, or ignition stage times, defined here as t_1 . Typical ignition stage times ranged from about 6 ms to about 1.5 ms. In Fig. 14, the data shown is for the conditions in which both stage 1 and stage 2 combustion were completed within the post flame region. As the figure indicates, the ignition time was relatively insensitive to oxygen mole fraction under these conditions. At the lower oxygen mole fraction conditions, $X_{O_2} \leq 0.15$, stage two combustion was either not completed or not even achieved at the lower temperature conditions. For $X_{O_2} = 0.1$ stage two combustion was not achieved until temperatures approached 1800 K. Table 2 provides a summary of which test conditions achieved and completed both stages of combustion. Temperature was found to have a dramatic effect on the ignition time, for example t_1 decreases by more than a factor of 2 with an increase of about 200 K in burner temperature. Other studies have shown that the presence of water vapor can greatly alter the ignition process of boron [2,11]. In this study oxygen mole fraction was the primary variable investigated, and the amount of water vapor in the burner combustion products was relatively constant. Fig. 14 also shows a comparison of ignition time measurements made by Yeh and Kuo [5] for 2–3 μm boron particles, which shows that the ignition times for the different particle sizes are relatively independent of size. The most likely reason for the lack of size dependence can be attributed to a combination of two issues, (1) particle ag-

glomeration, and (2) elemental or pure content of the particles. As our previous measurements showed, our size distribution can be represented by a log-normal distribution. From Eq. (3) we can extract the mass mean diameter, which is defined in Eq. (5).

$$d_{mm} = \frac{\sum n_i D_i^4}{\sum n_i D_i^3} \quad (5)$$

The mass mean diameter was selected as the appropriate scale rather than the geometric mean diameter since the emission intensity scales as a function of D^3 . Given that the aerosol follows a log-normal distribution, the majority of the mass of the particles will come from the upper “tail” of the distribution. More than 90% of the particles in the distribution are less than or equal to 679 nm. Thus we can reasonably conclude that the emission detected is well represented by the selection of the mass mean diameter.

When comparing the ignition time data of this study to that of Yeh and Kuo's [5] we must take into account the elemental or pure boron content of the particles. Since the primary particles making up the agglomerates in this study are on the nanoscale, the oxide shell thickness takes up a much larger fraction of the volume/mass of the particles. This means that our 679 nm agglomerates are only comprised of 72% by weight pure boron, which is not representative of a typical particle in that size range. For instance, SB Boron Corporation also sells a product named SB95 which is measured by Fisher sub-sieve sizer (FSSS) as being 700 nm in size and has an elemental content of 95–97%. In the case of Yeh and Kuo's [5] data, they used particles that ranged from 2–3 μm in size and estimated that the oxide layer thickness was 20 nm. This would result in particles having about 87% by weight pure boron. If we consider an idealized case in which the agglomerates under consideration in this study can be represented by a single spherical particle, this would result in an oxide layer thickness of about 34 nm, or more than 50% thicker than that of Yeh and Kuo's [5]. Furthermore, if we consider the volume that the oxide layer would occupy in each particle and then calculate the mass of each oxide layer we find that they are of the same order of magnitude (1.1×10^{-13} grams for our agglomerates compared to 6.1×10^{-13} grams for Yeh and Kuo's [5] particles). Since by definition the first stage of combustion is not completed until all of the oxide layer has been removed and the agglomerates studied here have a comparable oxide shell to that of Yeh and Kuo's [5], it is not surprising that the ignition times are quite comparable as well.

Since the primary variable affecting the ignition times was temperature an analytical expression to describe the ignition time was developed based upon an energy balance. The analysis assumed that the lumped capacitance assumption was appropriate, i.e. the temperature of the particle was spatially uniform at any instant during a transient process. In order to verify the validity of the

Table 2
Summary of results.

Test condition	Product mole fractions				Average burner temperature (K)	Stage 1 reached	Stage 2 reached	Stage 2 completed
	O ₂	H ₂ O	CO ₂	N ₂				
1	0.200	0.234	0.117	0.450	1684	yes	yes	yes
2	0.200	0.266	0.133	0.400	1808	yes	yes	yes
3	0.200	0.300	0.150	0.350	1854	yes	yes	yes
5	0.200	0.234	0.117	0.450	1637	yes	yes	yes
6	0.300	0.200	0.100	0.400	1630	yes	yes	yes
7	0.300	0.233	0.117	0.350	1797	yes	yes	yes
8	0.300	0.267	0.133	0.300	1872	yes	yes	yes
9	0.300	0.200	0.100	0.400	1578	yes	yes	yes
10	0.150	0.267	0.133	0.450	1718	yes	yes	yes
11	0.150	0.267	0.133	0.450	1814	yes	yes	yes
13	0.150	0.267	0.134	0.449	1596	yes	yes	no
14	0.100	0.233	0.117	0.550	1614	yes	no	no
15	0.100	0.267	0.134	0.499	1712	yes	no	no
16	0.100	0.267	0.134	0.499	1791	yes	yes	yes

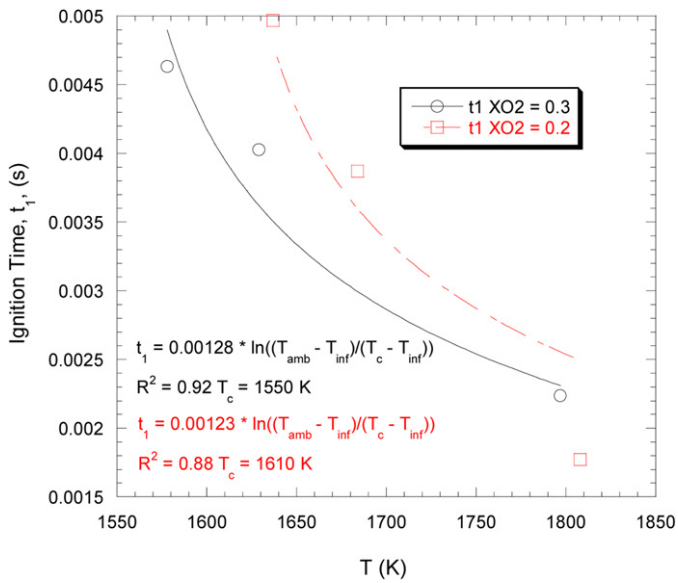


Fig. 15. Correlation for ignition time, t_1 .

lumped capacitance method, the Biot number, should be much less than unity. In this case the typical Biot number was approximately 0.005, thus validating the lumped capacitance assumption.

The energy balance for the particle is given by

$$\dot{E}_{st} = \dot{E}_{in} - \dot{E}_{out} + \dot{E}_{gen}, \quad (6)$$

where \dot{E} refers to the rate of change of energy, and the subscripts st, in, out, and gen refer to stored, in, out, and generated respectively. In this analysis, we assume that heat release due to chemical reaction is negligible until the point of ignition. Since the convective heat flux was typically three orders of magnitude larger than that of the radiation heat flux, we neglected radiation terms. With those simplifications, the energy balance reduces to only the storage term and a convective term as an energy input:

$$\dot{E}_{st} = \dot{E}_{in} \Rightarrow \rho_p V C_p \frac{dT}{dt} = h_\infty A_s (T - T_\infty). \quad (7)$$

The solution for which is given by Eq. (8).

$$t = \frac{\rho_p D_p C_p}{6h_\infty} \ln\left(\frac{T_{initial} - T_\infty}{T_c - T_\infty}\right). \quad (8)$$

From this analytical solution a correlation was developed (seen in Eq. (9)) for the ignition times for the two highest oxygen mole fraction conditions, $X_{O_2} = 0.2, 0.3$, in which the constants were lumped together into one “time constant,” τ_c , and T_c is the critical temperature to complete ignition in the burner. Fig. 15 shows the results of the correlation. Critical temperatures were 1610 K and 1550 K for $X_{O_2} = 0.2, 0.3$ respectively. We estimate the uncertainty of the critical temperatures at ± 40 K. This results in a sensitivity of Eq. (9) less than 10% at the higher temperatures and approximately 30% on the lower temperature end. These temperatures are consistent with previously observed ignition temperatures for larger sized boron [2,6,7,11]. Unlike nano-aluminum, which has been shown to ignite at lower temperatures than micron-sized aluminum, no such phenomenon was observed here.

$$t_1 = \tau_c \ln\left(\frac{T_{initial} - T_\infty}{T_c - T_\infty}\right). \quad (9)$$

Fig. 16 shows a summary of the results for the second stage burning times, t_2 , obtained in this study. On the burning time, t_2 , axis (Y-axis) the error bars represent our estimate for the uncertainty in the burning time. In this case this takes into account

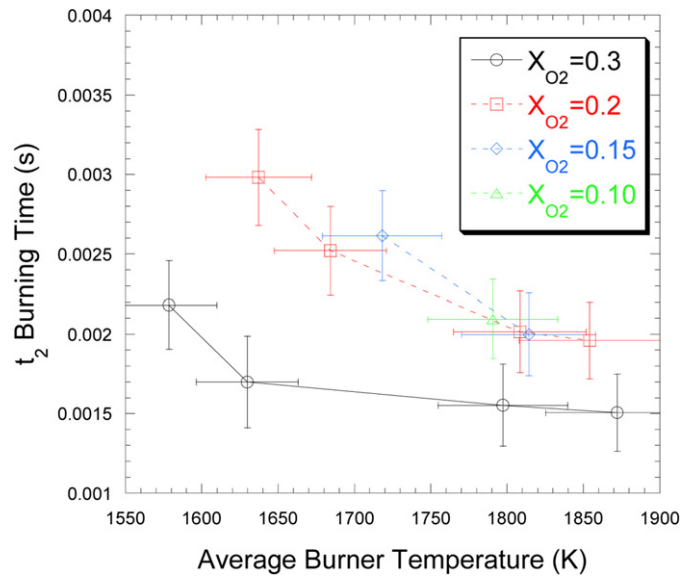


Fig. 16. t_2 burning times for SB99.

uncertainty in the piece-wise velocity profile used for the particle velocity as well as the spatial error detected in our emission images. For example when using the 95% area rule to determine burning time we selected ± 1 pixel for spatial resolution. Therefore the velocity profile determined the uncertainty in the particle velocity and the ± 1 pixel was selected as the spatial resolution. The two combined then determined the burning time uncertainty. Typical burning times range from about 3 ms down to about 1.5 ms. Oxygen mole fraction, X_{O_2} , had a clear effect on the burning time particularly at the lower range of the temperatures examined in this study. For example the burning time at a temperature of about 1625 K was approximately 50% longer for $X_{O_2} = 0.2$ than for $X_{O_2} = 0.3$. As the temperature was increased, the effect of X_{O_2} was less pronounced although there was still a significant difference between the two highest oxygen mole fractions, 0.2 and 0.3. For $X_{O_2} \leq 0.2$ there was no clear effect of oxygen mole fraction on the second stage burning time. However, the effect of temperature became more pronounced at low X_{O_2} . In the case of $X_{O_2} = 0.15$ at the lowest temperature condition second stage combustion was not completed before the flow left the burner area. For $X_{O_2} = 0.1$, second stage combustion was not even reached at all except for the highest temperature condition.

Fig. 17 shows a comparison of the t_2 burning times obtained in this study with those obtained with larger particles in other studies [2,4,5,24]. The data collected by Macek [2,4] used particles ranging from about 30 μm to 100 μm . The data from Li and Williams [24] came from 7 and 10 μm boron particles, while the data from Yeh and Kuo [5] came from particles that were 2–3 μm . Again, the data collected in this study was plotted considering its mass mean diameter, 679 nm, which was determined by extrapolating Eq. (3).

Here, a modified burning time, the product of oxygen mole fraction and burning time ($X_{O_2} t_2$), is plotted against particle size. These coordinates were chosen since both kinetic and diffusion limited reaction times are inversely proportional to X_{O_2} , therefore the product of $X_{O_2} t_2$ should be approximately independent of X_{O_2} , and should only be dependent on pressure and particle size [24].

From Fig. 17 it can be seen that the burning time of the largest particles studied by Macek [2,4] are dependent on the particle diameter by a factor of approximately 2, which would be consistent with diffusion limited burning, or the D^2 -law. The intermediate sized particles studied by Li and Williams [24], and Yeh and Kuo [5] have burning times that approach the kinetic limited regime

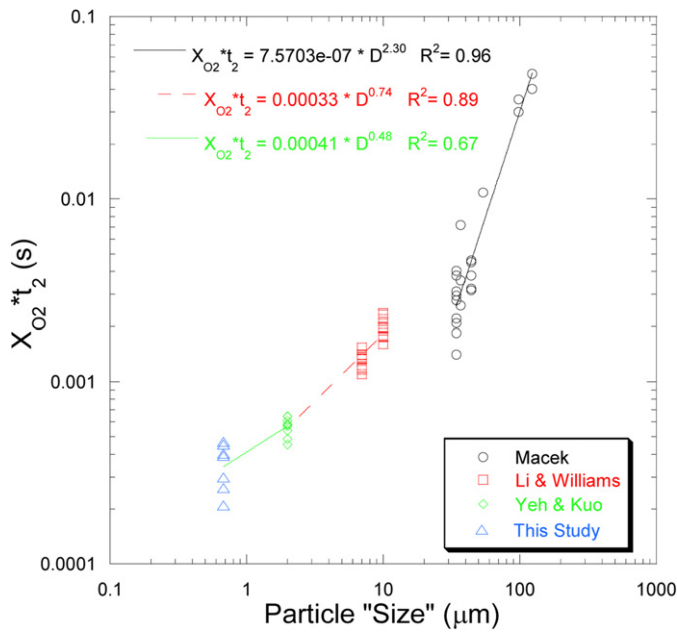


Fig. 17. t_2 burning time comparison to larger particles.

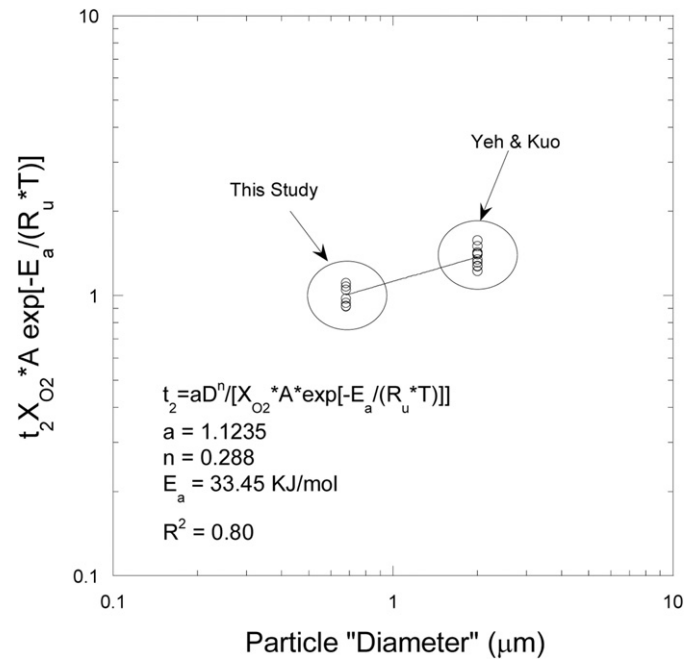


Fig. 19. t_2 burning time correlation.

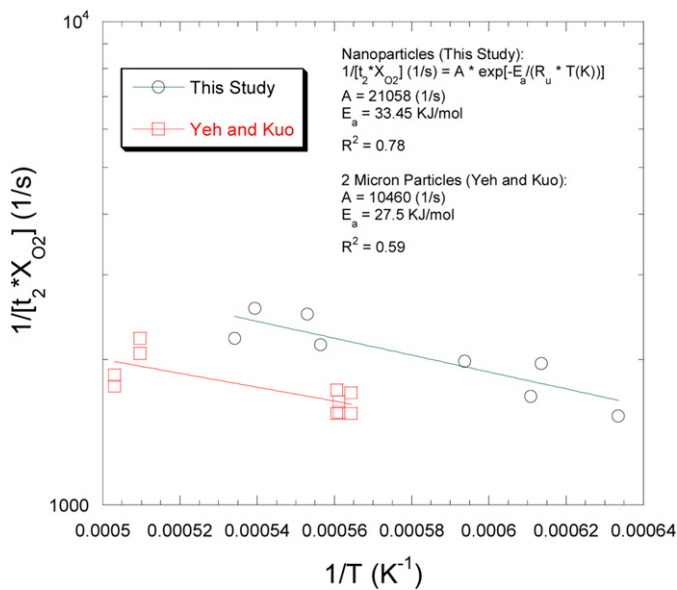


Fig. 18. t_2 Arrhenius burning rate law for SB99.

where the burning time follows a D^{-1} -law. As the size of the particles continue to decrease into the nanometer range, the particle size dependence continues to decrease, to well below unity ($t_b \sim D^{0.48}$), beyond what traditional theories have explained. The selection of another size scale such as the count mean or the geometric mean diameter only decreases the size dependence further.

In order to investigate whether or not boron nanoparticles exhibit significantly different properties than micron-sized particles, as nano-aluminum has, an Arrhenius burning rate law was obtained by plotting the reciprocal of the modified burning time with the reciprocal of burner temperature in Fig. 18. For comparison purposes, Yeh and Kuo's [5] data has also been plotted in the same manner. In this case, only the data collected for $X_{O_2} = 0.2$ and 0.3 have been included so that the conditions could be most comparable to the Yeh and Kuo [5] data. In this range, the activation energies between the two studies, and two very different particle sizes, are comparable considering experimental error and data

scatter. This is in great contrast to similar data for nano-aluminum. For instance, Park et al. [14] found that the activation energy of aluminum significantly decreases with decreasing particle size.

The Damköhler number analysis of Yeh and Kuo [5] suggests that the burning of these boron nanoparticles should be kinetically controlled. Huang et al. [30] proposed a burning time correlation based on a kinetically controlled system in the form of equation 10 for nano-aluminum. This correlation was applied to the present data set using the Arrhenius parameters obtained above, the results of which can be seen in Fig. 19.

$$t_2 = \frac{aD^n}{X_{O_2} A \exp\left(\frac{-E_a}{R_u T}\right)} \quad (10)$$

The correlation takes the activation energy determined for the nanoparticles in this study, and ranges from the nanoparticle data collected in this study up through the data collected by Yeh and Kuo [5] and can be seen in Fig. 19. This correlation reduces some of the scatter seen in the correlations developed earlier. With the Arrhenius parameters included, the size dependence decreases even further to $t_b \sim D^{0.29}$. Therefore, only a small benefit in burning time was obtained when going from 2–3 μm down into the nanometer range for boron. The nano-aluminum data correlated by Huang et al. [30] resulted in a size dependence of approximately $t_b \sim D^{0.3}$. Similarly, Bazyn et al. [16] found a size dependence $t_b \sim D^{0.6}$ for nano-aluminum at higher pressures.

Traditional burning rate theories, i.e. diffusion or kinetic limited schemes generally apply to a droplet, or single particle. In this case however, agglomerates are being introduced into the post flame region. Similarly the data correlated by Huang et al. [30], likely suffered from agglomeration. The effects of agglomeration are not well understood at this point. Heat transfer estimates, namely Biot number estimates, suggest that the entire agglomerate should be at a uniform temperature. Li and Williams [24] performed a heat transfer analysis that suggested that as the particle size and partial pressure of oxygen were decreased that boron particles might extinguish. The data collected in this study does not indicate particle extinguishment. If particle extinguishment were occurring, we might expect to observe shorter burn times at the lower temperatures, yet our data shows that the combustion time decreases with increasing temperature which is what would be expected for

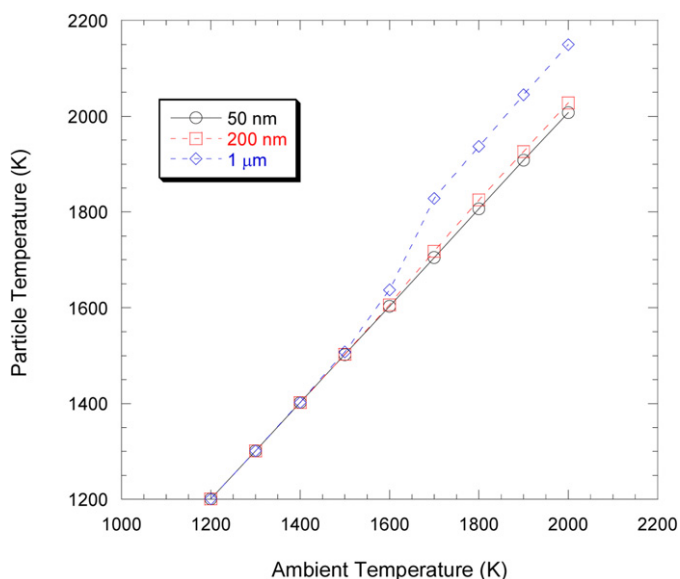


Fig. 20. Effect of ambient temperature on particle surface temperature.

a boron particle which is being completely consumed. A similar heat transfer analysis has been applied here. However, instead of specifying a particle surface temperature and solving for a quenching diameter as Li and Williams [24] did, here the particle surface temperature was solved for directly by solving the energy balance given in Eq. (11) (using Li and Williams' notation).

$$Q_5 \omega_5 = \frac{2k(T_p - T_\infty)}{D_p} + \varepsilon \sigma (T_p^4 - T_\infty^4). \quad (11)$$

The term on the left hand side of Eq. (11) refers to the heat released by the surface reaction given in Eq. (12), while the terms on the right hand side of Eq. (11) refer to the convective and radiative heat transfer. ω_5 is the kinetic rate constant for the surface reaction the values of which are temperature dependent and can be found in Ref. [24]. For the purpose of the analysis the oxygen mole fraction was assumed to be 0.2.

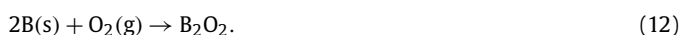


Fig. 20 shows the results of this analysis for several particle sizes. Clearly, the calculations suggest that the particle (or agglomerate) temperature will be very close to the ambient temperature for very small particles, which in this case is well below the melting temperature of pure boron ($T_m \sim 2340$ K). As the particle size becomes small, the heat generation cannot overcome the heat losses due to radiation and convection, therefore the particle surface is essentially limited to the ambient temperature. It is not until the particle size approaches $1 \mu\text{m}$ that the heat generation can significantly heat the particle above the ambient temperature. Once the particle size approaches $2 \mu\text{m}$, the particle surface temperature reaches the melting temperature of pure boron. This result demonstrates a significant difference in the burning behavior of the particles used in this study compared to those other researchers [2–5,24] and may help to explain the deviation from traditional theory on size dependence. Although the particles under question in this study are in agglomerated form, once the oxide shell has been removed the remaining boron is in solid phase. Whereas, considering Yeh and Kuo's [5] data, once the oxide layer has been removed, the remaining boron is in liquid phase. The increased particle temperature of larger particles due to heat generation overcoming convective and radiation losses at these lower ambient temperatures would certainly enhance both kinetic and diffusion rates. Another potential explanation for the deviation from traditional theory on size dependence is that this could be an artifact of agglomeration. Once

the agglomerate is heated up, the original oxide layer removed, and the pure "particle" begins to oxidize, the newly formed B_2O_3 may begin condensing onto or very close to neighboring particles within the agglomerate further restricting oxidation of pure material. Essentially this creates a situation in which there may never be a true second stage, i.e. clean boron combustion, but rather a mixture of stage 1 and stage 2 combustion throughout the consumption of the agglomerate. These two issues are the likely cause of the observed lack of size dependence in this study.

4. Conclusion

Ignition and burning time characteristics of nano-sized boron were studied in the post flame region of a flat flame burner. Unlike previous studies, the particles were injected in the transverse direction across the flame cross-section. Particle image velocimetry measurements coupled with ICCD images allowed for measurements of ensemble average ignition and burning time measurements of boron nanoparticles. The particles injected into the post flame region were agglomerates of smaller primary particles, with mean mass diameters of 679 nm. The effect of oxygen concentration and temperature were investigated.

Under appropriate temperature and oxygen mole fraction (X_{O_2}) conditions a two-staged combustion phenomenon was observed for the SB99 particles. Just after injection there was no visible signature of combustion, however, depending on flame conditions, a yellow/orange glow developed further downstream and was attributed to the first stage of boron combustion. The first stage of boron combustion, normally referred to as the ignition stage, is related the removal of the oxide (B_2O_3) layer. Following the first stage, a bright white glow zone was observed, and attributed to the second stage of boron combustion. The second stage combustion was considered full-fledged combustion of the "clean" pure boron particle.

The ignition stage time of nano-boron combustion, t_1 , was determined for a wide range of parameters, such as oxygen mole fraction X_{O_2} ranging from 0.1 to 0.3, and temperatures ranging from 1580 K to 1810 K. t_1 was found to be a strong function of temperature, but relatively insensitive to oxygen mole fraction in the ranges studied, while ranging from 1.5 ms at the highest temperatures, to about 6 ms at the lowest temperatures. When compared to available data from other researchers [5] employing micron-sized particles, the ignition stage of the boron nanoparticles was not substantially different from particles of approximately 2–3 μm in size. This is a result of the comparable initial oxide shell that is created by agglomerations of nano-sized particles whose elemental content of pure boron is significantly lower than those of larger particles.

Stage 2 combustion of boron nanoparticles was studied for $0.1 \leq X_{O_2} \leq 0.3$, and temperatures ranging from 1580 K to 1870 K. At the lowest temperatures, the oxygen mole fraction played a large role in the t_2 burning time and affected the ability of the particles to achieve stage 2 combustion. For $X_{O_2} \geq 0.2$ stage 2 combustion was achieved for temperatures as low as 1578 ± 31 K. At the lowest temperature condition, and $X_{O_2} = 0.15$, stage two combustion was achieved but was not completed while the particles remained in the post flame region of the burner. For $X_{O_2} = 0.1$, and the two lowest temperatures conditions, second stage combustion was not achieved while the particles were in the post flame region. Comparison with other researchers data revealed that the t_2 burning times did not follow a diffusion limited D^2 -law or a kinetic limited D^1 -law. Instead the t_2 burning time was found to be far less dependent on particle size than observations for larger particles. At this point we believe that this is a result of a significant difference in particle temperature between sub-micron-sized particles and micron-sized particles due to heat losses by

convection and radiation. Below 2000 K, particles below 1 μm are unable to generate enough heat to melt the pure material. Whereas larger boron particles (greater than 2 μm) are able to generate enough heat to be converted into liquid phase at temperatures near 2000 K. This observation may also be related to effects of particle agglomeration, and further studies are certainly warranted particularly at higher temperatures. An Arrhenius burning rate law was obtained which showed that the measured activation energy of the particles was consistent with other data [5] employing micron-sized particles. Similarly, the temperature range in which ignition was obtained for the nanoparticles was consistent with that of larger boron particles.

Acknowledgments

This research effort was sponsored through (A) Center for Energetic Concepts Development (CECD); a collaborative effort between the Naval Surface Warfare Center – Indian Head Division (NSWC-IHD), and the University of Maryland (UMD) and (B) The Army Research Office. The authors would specifically like to thank Mr. Gary Prybyla, Mr. Kevin Gessner, Mr. Bob Kaczmerak, Mr. Chris Fawls, and Mr. Bob Kavetsky of NSWC-IHD, along with Dr. David Anand, director of the CECD at UMD.

References

- [1] A. Ulas, K.K. Kuo, *Combust. Flame* 127 (1/2) (2001) 1935–1957.
- [2] A. Macek, J.M. Semple, *Combust. Sci. Technol.* 1 (1969) 181–191.
- [3] A. Macek, J.M. Semple, *Proc. Combust. Inst.* 13 (1971) 859–868.
- [4] A. Macek, *Proc. Combust. Inst.* 14 (1972) 1401–1411.
- [5] C.L. Yeh, K.K. Kuo, *Prog. Energy Combust. Sci.* 22 (6) (1996) 511–541.
- [6] S. Yuasa, H. Isoda, *Combust. Flame* 86 (3) (1991) 216–222.
- [7] S.N. Pen'kov, in: K.K. Kuo, R. Pein (Eds.), *Combustion of Boron Based Solid Propellants and Fuels*, CRC Press, Boca Raton, 1993, p. 218.
- [8] E.L. Dreizin, D.G. Keil, W. Felder, E.P. Vicenzi, *Combust. Flame* 119 (3) (1999) 272–290.
- [9] Y.I. Vovchuk, A.N. Zolotko, L.A. Klyachko, D.I. Polishchuk, V.G. Schevchuk, *Combust. Explos. Shock Waves* 10 (4) (1974) 538–540.
- [10] S.R. Turns, J.T. Holl, A.S.P. Solomon, G.M. Faeth, *Combust. Sci. Technol.* 43 (5/6) (1985) 287–300.
- [11] T. Yoshida, S. Yuasa, *Proc. Combust. Inst.* 38 (2000) 2735–2741.
- [12] R.A. Yetter, H. Rabitz, F.L. Dryer, *Combust. Flame* 83 (1/2) (1991) 43–62.
- [13] M.M. Mench, K.K. Kuo, C.L. Yeh, Y.C. Lu, *Combust. Sci. Technol.* 135 (1–6) (1998) 262–292.
- [14] K. Park, D. Lee, A. Rai, D. Mukherjee, M.R. Zachariah, *J. Phys. Chem.* 109 (15) (2005) 7290–7299.
- [15] T. Parr, C. Johnson, D. Hanson-Parr, K. Higa, K. Wilson, in: *JANNAF Combustion Subcommittee Meeting*, December, 2003.
- [16] T. Bazyn, H. Krier, N. Glumac, *Combust. Flame* 145 (4) (2006) 703–713.
- [17] G.A. Risha, E. Boyer, B.J. Evans, K.K. Kuo, in: *Materials Research Symposium*, Boston, MA, USA, 2003.
- [18] Y. Yang, S. Wang, Z. Sun, D. Dlott, *Propell. Explos. Pyrotech.* 30 (3) (2005) 171–177.
- [19] S.H. Kim, B.Y.H. Liu, M.R. Zachariah, *J. Colloid Interface Sci.* 282 (1) (2005) 46–57.
- [20] S.K. Friedlander, *Smoke, Dust, and Haze Fundamentals of Aerosol Dynamics*, 2nd ed., Oxford University Press, New York, 2000.
- [21] G. Young, R. Balar, K. Yu, in: *42nd Joint Propulsion Conference and Exhibit*, Sacramento, CA, USA, 2006, AIAA 2006-4401.
- [22] R.M. Mihalcea, D.S. Baer, R.K. Hanson, *Appl. Opt.* 36 (33) (1997) 8745–8752.
- [23] R.M. Mihalcea, D.S. Baer, R.K. Hanson, *Meas. Sci. Technol.* 9 (3) (1998) 327–338.
- [24] S.C. Li, F.A. Williams, in: K.K. Kuo, R. Pein (Eds.), *Combustion of Boron Based Solid Propellants and Fuels*, CRC Press, Boca Raton, 1993, p. 248.
- [25] R.O. Foelsche, R.L. Burton, H. Krier, *Combust. Flame* 117 (1/2) (1999) 32–58.
- [26] S.C. Li, F.A. Williams, F. Takahashi, *Proc. Combust. Inst.* 22 (1988) 1951–1960.
- [27] M.J. Spalding, H. Krier, R.L. Burton, *Combust. Flame* 120 (1/2) (2000) 200–210.
- [28] M.J. Spalding, H. Krier, R.L. Burton, in: *35th Aerospace Sciences Meeting and Exhibit*, Reno, NV, USA, 1997, AIAA 97-0119.
- [29] T. Bazyn, H. Krier, N. Glumac, *J. Propul. Power* 21 (4) (2005) 577–582.
- [30] Y. Huang, G.A. Risha, V. Yang, R.A. Yetter, *Proc. Combust. Inst.* 31 (2007) 2001–2009.